Thermodynamic Cycle Analysis of Superadiabatic Matrix-Stabilized Combustion for Gas Turbine Engines

Danyal Mohaddes[a,*], Clarence T. Chang[b], Matthias Ihme[a]

[a]*Department of Mechanical Engineering, Stanford University, California 94305, USA*
[b]*NASA Glenn Research Center, Cleveland, OH 44135, USA*

Abstract

In aircraft propulsion as well as stationary power generation, gas turbine engines remain a key energy conversion technology due to their high thermal efficiencies and low emissions. However, as emission requirements become increasingly stringent, engine manufacturers have sought to design combustion systems that operate near the fuel-lean limit of flammability. In this study, superadiabatic matrix-stabilized combustion, also known as porous media combustion, is evaluated as an advanced combustion concept for extending the lean flammability limit to achieve improved efficiency and emissions. To this end, a Brayton cycle analysis is developed and key parameters of the porous matrix are identified for maximizing the extension of the lean flammability limit. It is shown that stabilization of combustion below the nominal lean flammability limit allows for the design of engines with significantly higher pressure ratios and lower dilution ratios without increasing turbine inlet temperatures, thus improving cycle thermal efficiency. Combustor flammability limits were shown to be extendable by up to 32% when employing matrix-stabilized combustion, resulting in thermal efficiency gains of up to 11% compared to a nominal design.

Keywords: Superadiabatic combustion, Thermal efficiency, Brayton cycle, Porous media combustion, Gas turbine engines

Highlights

- Leaner combustion improves Brayton cycle efficiency, flammability limits hinder it
- Internal heat recirculation using porous media can extend lean flammability limit
- Analyzed gas turbine employing thermodynamic model of matrix-stabilized combustion
- Demonstrated thermal efficiency gains up to 11%, lean limit extension up to 32%
- Matrix-stabilized combustion can improve efficiency and emissions for gas turbines

*Corresponding author

Email addresses: danmohad@stanford.edu (Danyal Mohaddes), clarence.t.chang@nasa.gov (Clarence T. Chang), mihme@stanford.edu (Matthias Ihme)

1. Introduction

In aerospace propulsion as well as many electric power generating systems, the power plant of choice is the gas turbine engine operating on the Brayton cycle due to high thermal efficiency, mechanical reliability and rapid start-up times [1]. Manufacturers are under continuous pressure to improve thermal efficiency, which has been achieved primarily through increased pressure ratios and higher turbine inlet temperatures. To meet increasingly stringent regulatory requirements for emissions of carbon monoxide (CO) and oxides of nitrogen (NO_x) [2] while improving engine performance, a number of combustor designs have been proposed [3]. In stationary power generation applications employing natural gas as well as aviation engines employing TAPS (Twin Annular Premixing Swirler) systems [4], combustors operate in a lean premixed mode in a highly turbulent flow environment. This results in low NO_x production, but creates issues related to combustor stability, particularly those of blow-out and flashback.

Superadiabatic combustion and its application to gas turbine engines is the focus of this study. A concept first proposed by Hardesty and Weinberg [5], superadiabatic or 'excess enthalpy' combustion allows for the combustion of nominally non-flammable fuel-lean mixtures through internal heat recirculation. This internal heat recirculation is distinct from recuperating systems commonly used in thermal power plants, in that the final enthalpy of the product stream remains unchanged compared to that of the nominal system without any heat recirculation. Two intermediate stages are added to the combustion process: reactant preheating and product cooling by internal heat recirculation. Heat from the combustion products preheats the reactant stream, resulting in a combustion temperature exceeding the nominal adiabatic flame temperature and intermediate products thus termed 'superadiabatic'. The intermediate product stream is cooled to its final temperature by heat recirculation to the reactants. By the first law of thermodynamics, the enthalpy of the final product stream must equal that of the nominal system, since heat recirculation in this manner is internal to the combustor. However, since leaner mixtures require higher reactant temperatures for flammability [6], reactant preheating through superadiabatic combustion results in extension of the lean flammability limit, allowing the combustion of reactant mixtures of lower fuel-air equivalence ratios than otherwise possible. The present study employs this principle to improve the thermal efficiency of a Brayton cycle.

Stabilization of a flame within an inert porous matrix, also referred to as porous media combustion, was first proposed in [7] as a practicable means to achieve superadiabatic combustion and is the basis for many superadiabatic combustion systems, with diverse application areas including household cooking devices [8] and thermophotovoltaic power conversion [9]. Combustion in porous inert media has been the subject of comprehensive reviews [10] that should be consulted for in-depth description of the relevant physical processes; a brief overview is given here. An inert porous solid, typically made of sillicon carbide, alumina, or other heat-conducting ceramic material, is placed in the path of the reactant gas stream and a combustion reaction is stabilized within it. The combustion products heat the solid downstream of a thin combustion zone via convection. The solid matrix recirculates the heat upstream from the post-combustion region to the pre-combustion region via conduction and radiation. Incoming gases are then preheated by convection from the solid prior to entering the combustion zone. The stabilization of combustion within the thin zone is commonly accomplished with the interface-stabilized design [11], which consists of a step-change in porosity or pore diameter, although other stabilization methods have been proposed [12]. Flow through the matrix results in a small viscous pressure loss. The upstream segment has small pores to prevent flashback, whereas the downstream section has large pores to allow flame propagation. The pore-scale velocity is deterined by the void fraction ϵ, defined as the ratio of void area to total area in a given cross section of the matrix. The matrix is designed such that for a range of operating conditions the flame is stabilized at the interface between the two segments, with the flame propagating upstream from the large pore segment, but unable to propagate in the small pore segment owing to quenching and flow acceleration. The geometric properties of the matrix and the thermal and radiative properties of the matrix material determine the system's effectiveness in heat recirculation as well as the level of pressure loss. Figure 1 illustrates superadiabatic matrix-stabilized combustion schematically and through direct imagery of the experimental system described in [12]. Typical temperature profiles for the solid and gas phases are shown as well as axial locations corresponding to thermodynamic states, denoted Φ_i, considered in Sec. 4.

Matrix-stabilized combustion has been proposed as an alternative combustion concept for gas turbine engines [13]. As a stand-alone concept, matrix-stabilized combustion has been analyzed experimentally, theoretically, and numerically [14]. Novel applications and modifications of the Brayton cycle, such as augmentation with concentrated solar power [15], remain areas of active research. However, there remains a need to perform a systematic study of the effect of matrix-stabilized combustion on the performance of gas turbine engines operating on the Brayton cycle. To this end, the objective of this study is to develop a system-level model of matrix-stabilized combustion and conduct a thermodynamic cycle analysis of a gas turbine engine employing this technology. The effects of matrix-stabilized combustion on cycle efficiency and system design are studied parametrically, and matrix parameters key to cycle performance are identified.

The remainder of this manuscript is structured as follows. The Brayton cycle is analyzed in Sec. 2 to identify opportunities for efficiency improvement. Limitations to those opportunities due to stability considerations are described in Sec. 3. Section 4 develops a thermodynamic model for matrix-stabilized combustion and identifies key parameters affecting combustor performance. Effects of matrix-stabilized combustion on cycle performance are evaluated in Sec. 5, and some discussion of the analysis performed is given in Sec. 6. The manuscript closes with conclusions in Sec. 7.

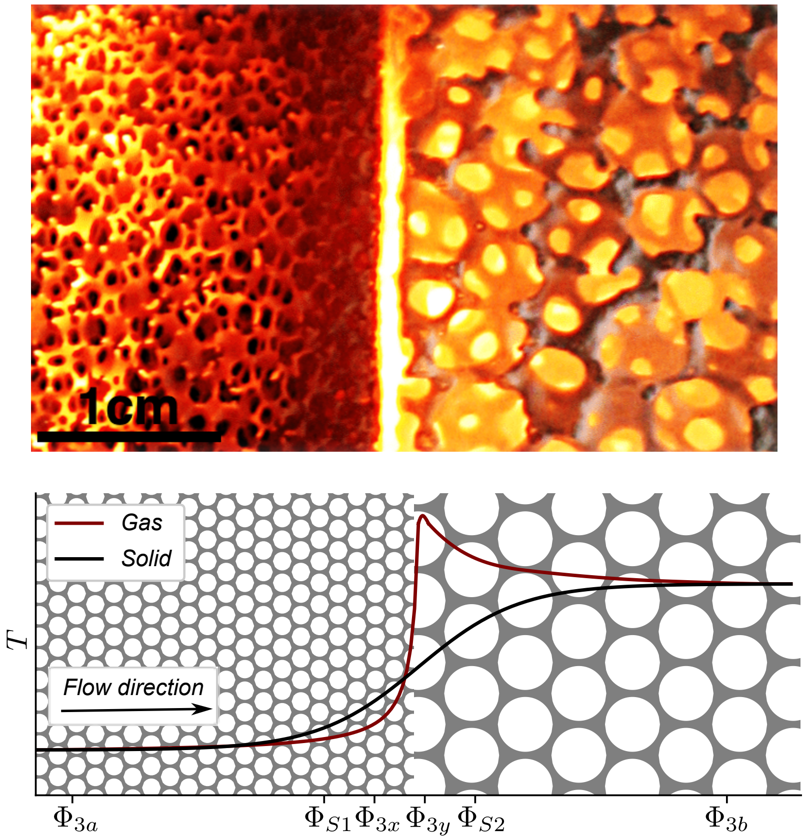

Figure 1: Depiction of superadiabatic matrix-stabilized combustion via schematic representation and direct imagery. Top: Direct imagery [16] of a flame stabilized inside a silicon carbide porous matrix [12] with flow from left to right. The upstream section is 65PPI (pores-per-inch) and downstream is 10PPI, with a total burner length of 76mm of which approximately 40mm is shown in the figure. Light emission is due primarily to radiation from the solid phase. Bottom: Schematic representation of solid and gas-phase temperatures in superadiabatic matrix-stabilized combustion employing the interface-stabilized design.

2. Brayton Cycle Analysis

2.1. Cycle Description

A stationary gas turbine engine employing fuel-lean premixed combustion is analyzed. This analysis is readily extendable to turbojet and turbofan propulsion engines by considering effects of bypass ratio and operation with liquid fuels. Figure 2 shows the mass and energy flows associated with the system considered. Thermodynamic state vectors are denoted $\Phi_i = [T_{ti}, p_{ti}]^T$, where the subscript i refers to the stations in Fig. 2. The subscript t denotes stagnation conditions; its omission indicates static conditions. The cycle description developed and the system boundaries considered for individual components follow that of [17].

Sea-level ambient air enters the engine at Φ_2 at a mass flow rate $\dot{m}_2$ and undergoes polytropic compression with a pressure ratio $\pi_c \equiv p_{t3}/p_{t2}$ and adiabatic efficiency η_c to Φ_3 at a rate $\dot{m}_3$, where $\dot{m}_3 = \dot{m}_2$. Part of

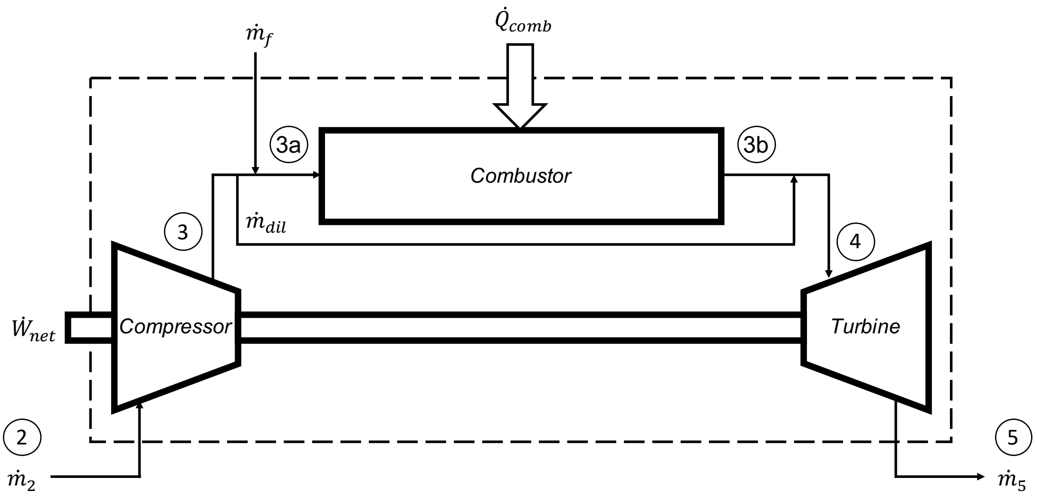

Figure 2: Mass and energy flows for an open Brayton cycle. Dashed line shows system boundary.

the compressed air stream is diverted around the combustor according to the dilution ratio β,

$$\beta = \frac{\dot{m}_{dil}}{\dot{m}_3}, \tag{1}$$

where $\dot{m}_{dil}$ is the mass flow rate of air in the dilution stream. Fuel is mixed with the main air stream at a rate $\dot{m}_f \ll \dot{m}_3$ prior to the combustor inlet state Φ_{3a}. Changes in stagnation enthalpy due to fuel addition are neglected, such that a premixed stream enters the combustor at a rate $\dot{m}_{3a} = \dot{m}_3 + \dot{m}_f - \dot{m}_{dil}$ with $T_{t3} = T_{t3a}$. The combustion process is modeled as isobaric heat addition at a rate

$$\dot{Q}_{comb} = \dot{m}_f LHV, \tag{2}$$

where LHV is the lower heating value of the fuel. It is assumed that β and $\dot{m}_f$ are sufficiently small such that the combustor equivalence ratio $\phi_{loc} < 1$, with

$$\phi_{loc} = \frac{\phi}{1-\beta}, \tag{3}$$

and $\phi = f/f_{st}$ is the global equivalence ratio, $f = \dot{m}_f/\dot{m}_3$ is the global fuel-air ratio, and the subscript st denotes the stoichiometric condition. The equivalence ratio within the combustor ϕ_{loc} is thus increased from its global value ϕ due to the presence of the dilution duct. Flow through the combustor results in a pressure drop according to the pressure ratio $\pi_b \equiv p_{t3b}/p_{t3a}$ and is attributable largely to the flow acceleration needed for flame stabilization through turbulence, as well as the Rayleigh loss across the deflagration wave [3]. The dilution air stream is mixed with the combustion products prior to entering the turbine at state Φ_4 to reduce the turbine inlet temperature T_{t4}. The diluted product stream enters the turbine at a rate $\dot{m}_4 = \dot{m}_3 + \dot{m}_f$. Work is extracted through polytropic expansion in the turbine according to a pressure ratio $\pi_t \equiv p_{t4}/p_{t5} = \pi_c \pi_b$ and adiabatic efficiency η_t prior to exhausting to the ambient environment at Φ_5

at a rate $\dot{m}_5 = \dot{m}_4$. It is assumed the exhaust stream is fully expanded such that $p_{t5} = p_{t2}$. Part of the extracted work drives the compressor, the rest being available as output $\dot{W}_{net}$. The cycle thermal efficiency η_{th} is thus computed as

$$\eta_{th} = \frac{\dot{W}_{net}}{\dot{Q}_{comb}} \tag{4}$$

where $\dot{W}_{net} = \dot{W}_t - \dot{W}_c$ is the difference between turbine and compressor power, with

$$\dot{W}_c = \dot{m}_3 \left(h_{t3} - h_{t2}\right) \tag{5a}$$

$$\dot{W}_t = \left(\dot{m}_3 + \dot{m}_f\right)\left(h_{t4} - h_{t5}\right) \tag{5b}$$

where h_{ti} denotes stagnation enthalpy at state Φ_i.

2.2. Effect of Changing Equivalence Ratio on Cycle

The effect of varying ϕ on the Brayton cycle is examined due to its consequences for cycle efficiency and its limitations due to flammability, as will be discussed in Sec. 3. Material considerations typically limit the turbine inlet temperature to a maximum of 1800K [18] and T_{t4} is thus considered a constant design parameter. For a given compressor inlet state $\Phi_2 = \Phi_{amb} = [300\text{K}, 101325\text{Pa}]^T$, all others can be determined uniquely as a function of design parameters $\psi \equiv [T_{t4}, \beta]^T$, component performance parameters $\zeta \equiv [\eta_c, \eta_t, \pi_b]^T$, gas thermo-chemical properties $\xi \equiv [c_p, c_v, LHV]^T$ and ϕ expressed in terms of the fuel-air ratio f. The values c_p and c_v are the isobaric and isochoric heat capacities of air. Assuming air to be a calorically perfect gas, neglecting the effect of the fuel vapor on the mixture thermodynamic properties and assuming constant component performance parameters, then $\psi = \text{const}$, $\zeta = \text{const}$, $\xi = \text{const}$, stagnation enthalpy may be expressed as $h_{ti} = c_p T_{ti}$ and the remaining state variables determined as

$$T_{t3} = T_{t4} - \frac{f}{f+1}\frac{LHV}{c_p} \tag{6a}$$

$$\pi_c = \left\{1 + \eta_c \left[\frac{1}{T_{t2}}\left(T_{t4} - \frac{f}{f+1}\frac{LHV}{c_p}\right) - 1\right]\right\}^{\frac{\gamma}{\gamma-1}} \tag{6b}$$

$$T_{t5} = T_{t4}\left[1 - \eta_t\left(1 - \left(\pi_c \pi_b\right)^{\frac{1-\gamma}{\gamma}}\right)\right] \tag{6c}$$

where $\gamma \equiv c_p/c_v$. Using the properties of air, c_p and γ vary less than 14% and 9% across the range of temperatures and pressures present in the cycle, and thus the assumption of a calorically-perfect gas is found to be reasonable for the present study. Figure 3 shows the effect of ϕ on the temperature/entropy and pressure/specific-volume diagrams for a Brayton cycle. Values used in ψ, ζ and ξ are noted in Table 1 and are typical for small stationary gas turbine engines operating using methane fuel at sea-level ambient conditions [19]. The calculation of β is discussed in Sec. 3.1. Unless otherwise stated, these values will be used for subsequent calculations. Figure 3a shows that with decreasing ϕ, the combustor inlet temperature T_{t3} increases to maintain a constant turbine inlet temperature T_{t4}. This temperature increase is accomplished by increasing the compressor pressure ratio π_c, as seen in Fig. 3b.

ϕ_0	ψ		ζ			ξ		
$[-]$	T_{t4} [K]	β $[-]$	η_c $[-]$	η_t $[-]$	π_b $[-]$	c_p [J/(kg·K)]	c_v [J/(kg·K)]	LHV [MJ/kg]
0.3	1400	0.1	0.9	0.9	0.95	1200	860	50.1

Table 1: Constants used in Brayton cycle calculations.

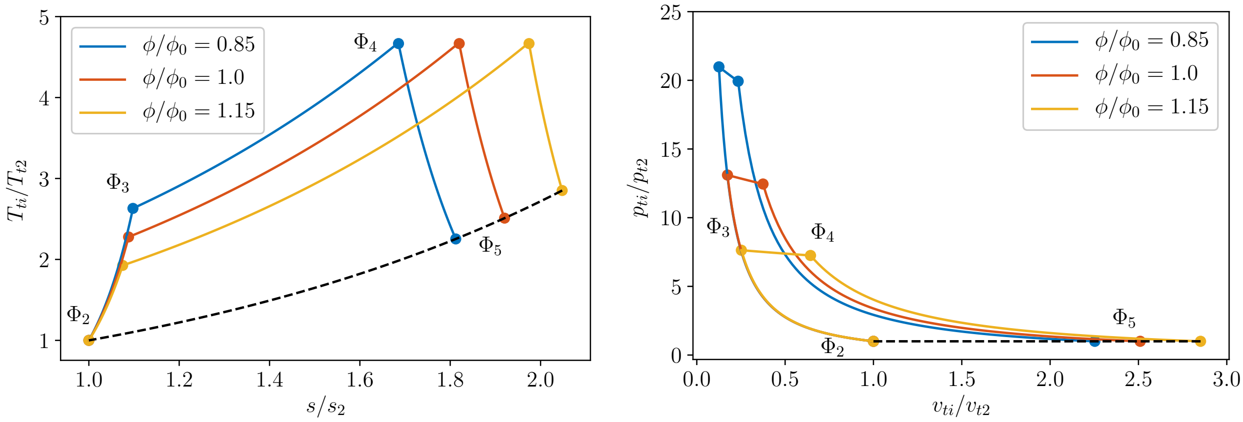

(a) $T - s$ diagram

(b) $p - v$ diagram

Figure 3: Effect of changing global equivalence ratio ϕ while maintaining a constant turbine inlet temperature T_{t4} on Brayton cycle. Dashed line indicates open cycle isobaric cooling.

2.3. Effect of Changing Equivalence Ratio on Thermal Efficiency and Emissions

The effect of ϕ on engine performance is demonstrated by computing the cycle thermal efficiency η_{th}. From Eqs. 4–6

$$\eta_{th} = \frac{c_p}{fLHV}\left[(1+f)\,\eta_t T_{t4}\left(1-(\pi_c\pi_b)^{\frac{1-\gamma}{\gamma}}\right) - \frac{T_{t2}}{\eta_c}\left(\pi_c^{\frac{\gamma-1}{\gamma}}-1\right)\right]. \tag{7}$$

Increasing the turbine inlet temperature T_{t4} thus increases thermal efficiency, motivating the effort to push to higher temperatures [20]. Figure 4a shows the effect of ϕ on η_{th}, where η_c and η_t are considered parametrically. Reduction in ϕ results in increased cycle efficiency, and a maximum exists for non-ideal turbomachinery. Figure 4b shows that the increased efficiency is accompanied by a significant increase in compressor pressure ratio. The normalization values $\eta_{th,0}$ and $\pi_{c,0}$ are computed at ϕ_0 for the values of η_c and η_t shown in the figure, where $\eta_{th,0} = 0.4$ and $\pi_{c,0} = 15$ obtained for $\eta_c = 0.9$ and $\eta_t = 0.9$ are typical for stationary gas turbine engines [19].

Improvements in η_{th} have a direct impact on CO_2 emissions. Considering the major products of lean combustion, the mass flow rate of CO_2 in the engine exhaust $\dot{m}_{CO_2}$ is proportional to $\dot{m}_f$. From Eqs. 2 and

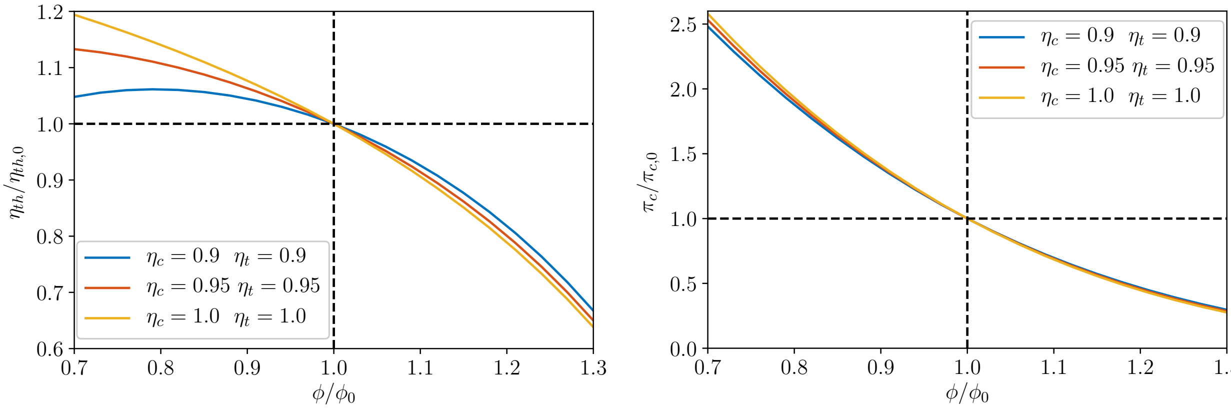

(a) Thermal efficiency, η_{th}

(b) Compressor pressure ratio, π_c

Figure 4: Effect of changing global equivalence ratio ϕ while maintaining a constant turbine inlet temperature T_{t4} on cycle performance.

4

$$\dot{m}_{CO_2} \sim \dot{m}_f = \frac{\dot{W}_{net}}{LHV\eta_{th}}. \tag{8}$$

For a constant power output, improved η_{th} thus results in reduced fuel consumption and correspondingly reduced CO_2 emissions. Also of concern, however, are emissions of NO_x and CO, whose quantitative prediction is notoriously difficult and strongly dependent upon combustor design [3]. Emissions from matrix-stabilized combustion systems are considered specifically in Sec. 5.4. Here, it is sought to capture the qualitative trends in emission profiles as a function of ϕ for a constant T_{t4} to further motivate operation at leaner conditions. To this end, the system was modeled between Φ_{3a} and Φ_{3b} using an isochoric perfectly-stirred flow reactor with Cantera [21], employing the GRI 3.0 chemical mechanism for methane combustion [22]. The reactant stream mass flow rate $\dot{m}_{3a}$ and combustor volume V were held constant while the reactant stream temperature T_{t3a} and system pressure p_{t3a} were varied in tandem with ϕ evaluated from Eqs. 6a and 6b. State variables inside the combustor were evaluated at stagnation conditions. The product stream composition was then considered for a range of ϕ, the results of which are shown in Fig. 5, where pollutant levels are expressed in terms of an emission index EI, defined for a pollutant species i as

$$EI_i = Y_i \frac{f+1}{f} \; [\mathrm{kg}_i/\mathrm{kg}_f]. \tag{9}$$

The values selected for $\dot{m}_{3a}$ and V were based on typical values for combustor mass flux $\dot{m}''_{3a}$ and residence time τ_{res} [23], although trends were found to be robust to variations in these values. From Eqs. 8 and 9, the exhaust mass flow rate of a pollutant i is

$$\dot{m}_i = EI_i \frac{\dot{W}_{net}}{LHV\eta_{th}}, \tag{10}$$

where the mass fractions Y_i were obtained from the perfectly-stirred flow reactor calculations. From this equation and considering Figs. 4 and 5, it can be seen that for a constant power output, a reduction in ϕ results in a reduction in both NO_x and CO emissions nearly independent of turbomachinery efficiency.

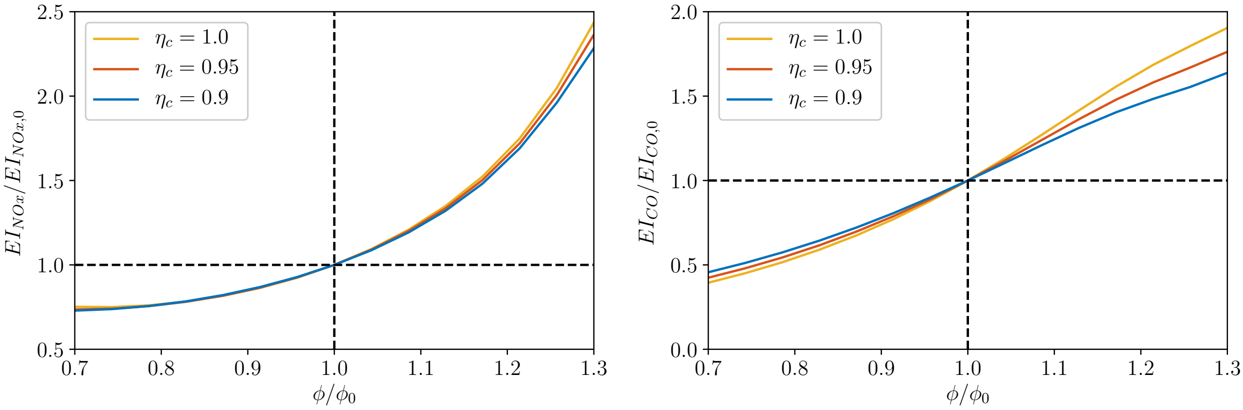

(a) NO_x emission index, EI_{NO_x}

(b) CO emission index, EI_{CO}

Figure 5: Effect of changing global equivalence ratio ϕ while maintaining a constant turbine inlet temperature T_{t4} on emissions for a gas turbine combustor without matrix stabilization. The nominal values $EI_{i,0}$ are the values of EI_i obtained at ϕ_0.

2.4. Summary of Cycle Analysis Assumptions

In the preceding description and subsequent analysis, a number of assumptions have been made for each component in the cycle. The system is assumed to be a stationary gas turbine engine operating according to an open Brayton cycle at steady-state and at sea-level ambient conditions. Air is taken as a calorically-perfect working fluid, with constant thermo-chemical properties throughout the cycle. The compressor has a pressure ratio π_c and operates with an adiabatic efficiency η_c. Part of the post-compressor air stream is diverted into the dilution duct with a constant dilution ratio β. Fuel-air mixing prior to the combustor is assumed isothermal at T_{t3a}. Combustion is modeled as heat addition, and is assumed fuel-lean and complete. Total pressure losses through the combustor are taken as constant with a pressure ratio $\pi_b = 0.95$. Heat losses are neglected throughout most of the analysis, but are considered specifically in Sec. 6.3. Mixing of the combustion product stream with the dilution stream is assumed adiabatic. The turbine operates with an adiabatic efficiency η_t and the exit state is fully-expanded, with a pressure ratio $\pi_t = \pi_c \pi_b$. Thermal efficiency is calculated based on net work output, neglecting mechanical losses. The effects of non-adiabatic compressor and turbine efficiencies are considered parametrically.

3. Combustor Stability Analysis

3.1. Lean Flammability Limit

The results of Sec. 2 suggest that efficiency and emissions can be improved by redesigning an engine to operate at a reduced ϕ with a corresponding increase in π_c. The naivety of such a strategy becomes apparent, however, when combustor stability is considered. In this work, combustor stability is considered in terms of the lean flammability limit (LFL) and the flashback limit; dynamic instabilities arising from thermo-acoustic effects are highly geometry-dependent and are outside the scope of this analysis.

To reduce emissions of NO_x and CO, engines employing lean premixed combustion are generally designed to operate near LFL, below which combustion is no longer self-sustaining and flame-out occurs. The flammability limits for a combustion reaction are determined by the chemical and physical properties of the reactants, their initial temperature and the system pressure [24]. For methane-air mixtures, LFL expressed as a fuel mole fraction $X_{f,LFL}$ is independent of pressure up to 25bar [25]. An empirical correlation [6] can thus be used to express LFL as a function of the unburned gas temperature,

$$X_{f,LFL} = CT_u^{-n}, \tag{11}$$

where T_u is the unburned gas temperature, C is a constant approximately equal to 0.9795 for gaseous methane in air, and $n = 0.51536$ is an empirical constant [6]. This correlation shows that increasing the reactant temperature decreases LFL. Rearranging Eq. 11 for $T_u = T_{LFL}$ and noting that

$$\phi = \frac{X_f}{\tilde{f}_{st}\left(1 - X_f\right)}, \tag{12}$$

the minimum unburned gas temperature required to achieve flammability at a given ϕ is

$$T_{LFL} = \left[C\left(\frac{1-\beta}{\phi\tilde{f}_{st}} + 1\right)\right]^{1/n}, \tag{13}$$

where $\tilde{f}_{st}$ is the molar stoichiometric fuel-air ratio. Consistent with the assumption that engines are designed to operate at LFL, the dilution ratio β was assumed to be such that $T_{t3a} = T_{LFL}$ for $\phi = \phi_0$. Setting $\phi_{loc} = \phi_{LFL}$, β is obtained from Eq. 3 as

$$\beta = \frac{\phi_{LFL}\left(T_{t3a}\right) - \phi_0}{\phi_{LFL}\left(T_{t3a}\right)}, \tag{14}$$

where ϕ_{LFL} is obtained from Eq. 11 after converting X_f to ϕ using Eq. 12, and yielding $\beta \approx 0.1$ for ζ and ξ as in Sec. 2. Considering the ratio of the stagnation combustor inlet temperature T_{t3a} and the minimum temperature for flammability T_{LFL} as a function of ϕ in Fig. 6, it is clear that although a reduction in ϕ results in an increase in T_{t3a} to maintain a constant T_{t4} as per Eq. 6, the increase is not enough to maintain flammability as T_{LFL} increases at a greater rate. As such, the basic redesign of a cycle to operate at a lower ϕ to exploit the efficiency gains shown in Fig. 4 will result in combustor instability and flame-out. LFL thus limits achievable cycle efficiency.

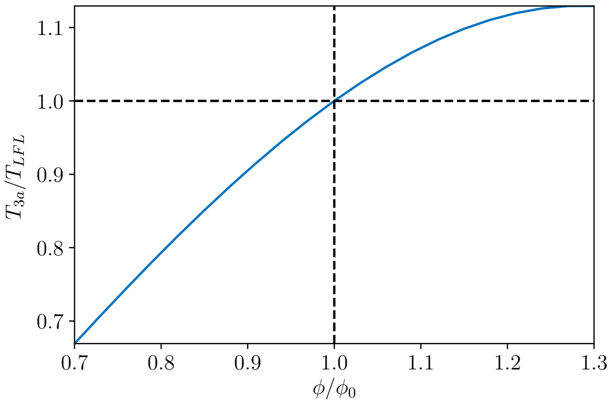

Figure 6: Effect of equivalence ratio ϕ on T_{3a}/T_{LFL} for a constant turbine inlet temperature T_{t4}. Conditions where $T_{3a}/T_{LFL} < 1$ result in flame-out.

3.2. Flashback due to Autoignition

In addition to flame-out, in lean premixed combustors, instability due to flashback must also be considered. Flashback of the flame into the mixing zone is determined by combustor geometry, inlet temperature and pressure, as well as fuel chemistry and ϕ [26]. Flashback may occur in a multitude of ways [27], but of particular importance is autoignition of the mixture prior to reaching the combustion zone [28]. Autoignition may be characterized by the ignition delay time τ_{ign}, here defined as the time required for the mixture to reach 99% of the adiabatic equilibrium temperature, and a characteristic flow time scale $\tau_{flow} \equiv L_c/u_{3a}$ with L_c being a characteristic length and u_{3a} the flow velocity at the combustor inlet. An ignition Damköhler number is defined as

$$Da_{ign} \equiv \frac{L_c/u_{3a}}{\tau_{ign}}. \tag{15}$$

The characteristic length scale is taken as the quenching distance d_q at the reference condition, and is obtained using the basic scaling relations [29] $d_q \sim \delta_f$ and $\delta_f \sim \alpha/s_L$, where δ_f is the flame thickness, α is the unburned mixture thermal conductivity, and s_L is the unstretched laminar flame speed. Noting that velocity can be obtained from mass flux as $u = \dot{m}''/\rho$ where ρ is the static density, then applying the ideal gas law at stagnation conditions and that $\rho_t/\rho = \left(1 + \frac{\gamma-1}{2} M_{3a}^2\right)^{\frac{1}{\gamma-1}}$, the flow velocity at the combustor inlet u_{3a} is evaluated as

$$u_{3a} = \dot{m}''_{3a} \frac{RT_{t3a}}{p_{t2}\pi_c} \left(1 + \frac{\gamma - 1}{2} M_{3a}^2\right)^{\frac{1}{\gamma-1}} \tag{16}$$

where $M \equiv u/c$ is the Mach number, c is the speed of sound, R is the gas constant of the fuel-air mixture, assumed equal to the nominal value for air $R = 287\text{J}/(\text{kg} \cdot \text{K})$, and $\dot{m}''_{3a}$ is the mass flux through the combustor, taken as $\dot{m}''_{3a} = 2.0\text{kg}/(\text{m}^2 \cdot \text{s})$ based on typical combustor geometries [23] and flow rates [17]. For typical gas turbine engine combustors, $M_{3a} < 0.3$ [3], and thus $\frac{\gamma-1}{2} M_{3a}^2 \ll 1$ such that Eq. 16 is approximated as

$$u_{3a} \approx \dot{m}''_{3a} \frac{RT_{3a}}{p_{t2}\pi_c}. \tag{17}$$

The ignition Damköhler number Da_{ign} is plotted as a function of ϕ in Fig. 7, where the flashback criterion due to autoignition is taken as $Da_{ign} \geq 1$. The autoignition time τ_{ign} was evaluated using an isobaric homogeneous reactor with Cantera [21] employing the GRI 3.0 chemical mechanism for methane combustion [22]. From Fig. 7, the effect of improved turbomachinery efficiency is to increase the flashback limit. However, even in the case of isentropic turbomachinery, the flashback limit is very low at $\phi/\phi_0 \approx 0.4$. Thus, for sufficiently lean mixtures, combustion instability may occur due to autoignition arising from the increased combustor inlet temperatures and pressures needed to maintain a constant T_{t4}, presenting another lean limit on ϕ in cycle design. Consideration of the potential gains in η_{th} with reduced ϕ described in Sec. 2 with the limitations imposed due to combustor stability detailed in this section motivates the integration of matrix-stabilized combustion in the Brayton cycle for LFL extension. A system-level model of matrix-stabilized combustion is thus needed to quantify its effects.

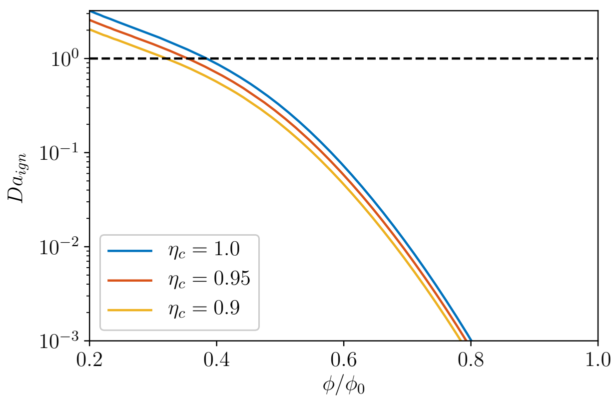

Figure 7: Effect of equivalence ratio ϕ on autoignition Damköhler number Da_{ign} for a constant turbine inlet temperature T_{t4}. The dashed line at $Da_{ign} = 1$ is taken as the limit of flashback due to autoignition.

4. Mathematical Model of Matrix-Stabilized Combustion

A steady-state, isobaric, thermodynamic model for combustion in a porous matrix integrated in a gas turbine engine is developed. As in the differential models of other authors [30], a two-phase system is considered, consisting of a gas phase and an inert solid. Heat is transported downstream by gas-phase convection and upstream by solid-phase conduction and radiation, neglecting gas-phase radiation. Interactions between the two phases occur through convective heat transfer; gas-solid radiation is neglected due to limited gaseous optical thickness [31]. The porous matrix is assumed to be insulated radially, such that axial radiative heat

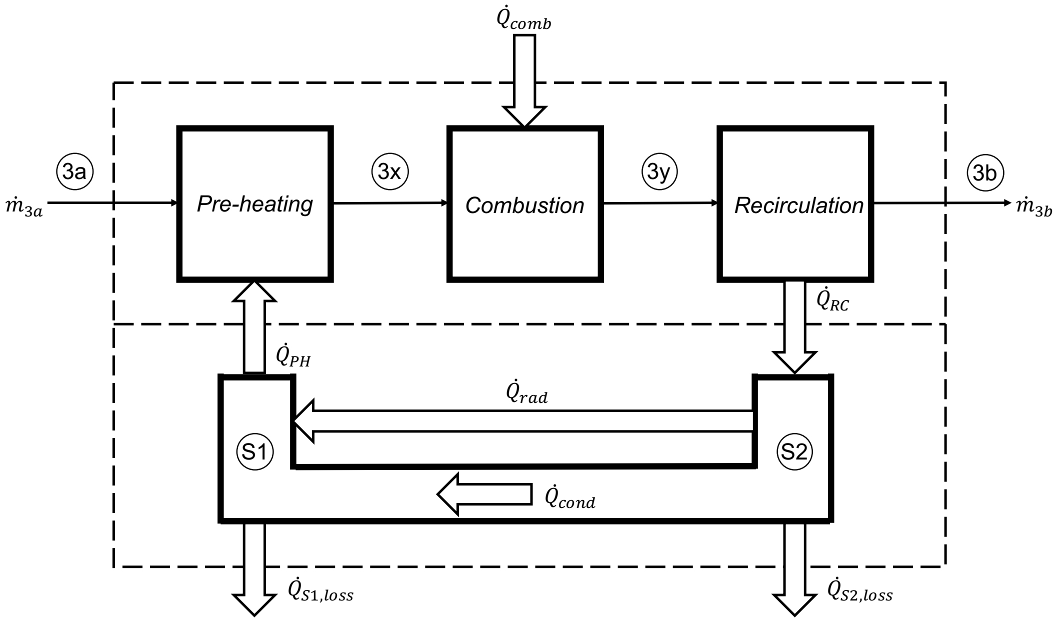

Figure 8: Thermodynamic model for superadiabatic matrix-stabilized combustion. Dashed lines indicate subsystem boundaries.

losses are considered, whereas radial heat losses are neglected. Effects of material degradation are also neglected.

Figure 8 illustrates the proposed model and the pathways for heat transfer within the system. As noted in the figure, the model describes the processes occurring between states Φ_{3a} and Φ_{3b} as defined in Fig. 2, where the mass flow through the system is $\dot{m}_{3a} = \dot{m}_{3b}$. Two new gaseous thermodynamic states are introduced, Φ_{3x} and Φ_{3y}, corresponding to the gas immediately prior to and after combustion, respectively. Two solid states, Φ_{S1} and Φ_{S2}, are introduced, which correspond to the solid temperature of the preheating and heat recirculation zones. Solid states are assumed to be fully described by a solid-phase temperature.

4.1. Gaseous Subsystem

In addition to the assumptions made regarding gas flow in Sec. 2, it is further assumed that combustion occurs in a thin zone within the matrix where heat transfer to and from the solid is negligible. Fuel-lean combustion is modeled as instantaneous isobaric heat release per Eq. 2. The first law of thermodynamics written between the four gaseous states inside the combustor, shown in Fig. 8, is

$$\dot{Q}_{PH} = \dot{m}_{3a} c_p \left(T_{t3x} - T_{t3a} \right) \tag{18a}$$

$$\dot{m}_f LHV = \dot{m}_{3a} c_p \left(T_{t3y} - T_{t3x} \right) \tag{18b}$$

$$-\dot{Q}_{RC} = \dot{m}_{3a} c_p \left(T_{t3b} - T_{t3y} \right) \tag{18c}$$

where $\dot{Q}_{PH}$ and $\dot{Q}_{RC}$ are the heat transferred from and to the solid by convection in the preheat and recirculation zones, respectively.

4.2. Solid Subsystem

Assuming steady-state heat transfer and no heat losses along the length of the matrix, an algebraic heat conduction equation can be written to describe heat transfer between Φ_{S1} and Φ_{S2}. Both radiative and conductive heat transfer are present, denoted $\dot{Q}_{rad}$ and $\dot{Q}_{cond}$, respectively. The Rosseland equation approximating radiation as a diffusive process [32] is used to express the solid-solid thermal radiative heat transfer in the porous media in terms of a temperature-dependent thermal conductivity,

$$\lambda_R = \frac{16\sigma T_S^3}{3K_R}, \tag{19}$$

where σ is the Stefan-Boltzmann constant, T_S is an average solid temperature, and K_R is the radiative extinction coefficient, which can be determined from the material and geometric properties of the porous matrix; here, Eq. 19 from [33] is employed. As in [31], heat conduction in the solid is expressed in terms of an overall thermal conductivity, λ_S

$$\dot{Q}''_{cond} = -\lambda_S \frac{\Delta T}{\Delta x} \tag{20}$$

where $\dot{Q}''_{cond}$ is the conductive heat transfer within the solid per unit cross-sectional area. Total heat transfer within the solid, $\dot{Q}_S = \dot{Q}_{cond} + \dot{Q}_{rad}$, is thus expressed as

$$\dot{Q}_S = \lambda_{S,eff} \frac{A_{CS}}{l} (T_{S2} - T_{S1}) \tag{21}$$

where A_{CS} is the matrix cross-sectional area, l is the matrix axial length, and $\lambda_{S,eff} = \lambda_S + \lambda_R$ is the effective thermal conductivity. Heat convected from the gas enters the solid subsystem at Φ_{S2} as $\dot{Q}_{RC}$, whereupon some heat is lost to the ambient by radiation from the end of the matrix as $\dot{Q}_{S2,loss}$. The same radiative heat loss mechanism is considered at the upstream end of the matrix at Φ_{S1}. Similar application of the first law at Φ_{S1} and Φ_{S2} yields

$$\dot{Q}_{PH} = \dot{Q}_S - \dot{Q}_{S1,loss}, \tag{22a}$$

$$\dot{Q}_{RC} = \dot{Q}_S + \dot{Q}_{S2,loss}. \tag{22b}$$

A simple model for steady radiative heat loss from the end sections of the matrix is employed,

$$\dot{Q}_{S1,loss} = \sigma\varepsilon_K (1-\epsilon) A_{CS} \left(T_{S1}^4 - T_{t3a}^4\right) \tag{23a}$$

$$\dot{Q}_{S2,loss} = \sigma\varepsilon_K (1-\epsilon) A_{CS} \left(T_{S2}^4 - T_{t4}^4\right) \tag{23b}$$

where ε_K is the gray-body emissivity of the porous material, ϵ is the void fraction of the porous matrix, and it is assumed that the upstream end of the matrix radiates to a surface at the combustor inlet temperature T_{t3a}, and the downstream end to a surface at the post-dilution turbine inlet temperature T_{t4}.

4.3. Final Equations

Combining the equations of Secs. 4.1 and 4.2 to perform an energy balance within the two-phase matrix-stabilized combustion system accounting for radiative heat losses to the surroundings, five equations are obtained for the five unknown state temperatures. Normalizing gas and solid temperatures with the ambient temperature $T_{t2} = 300\text{K}$ as $\theta_i = T_{ti}/T_{t2}$ and $\theta_{Si} = T_{Si}/T_{t2}$, respectively, and creating non-dimensional groups from the parameters of Secs. 4.1 and 4.2, the final non-dimensional equations are

$$\theta_{3x} - \theta_{3a} = \iota\left[\left(1+\delta\theta_S^3\right)\left(\theta_{S2}-\theta_{S1}\right) - \delta\mu_K\left(\theta_{S1}^4 - \theta_{3a}^4\right)\right], \tag{24a}$$

$$\theta_{3y} - \theta_{3x} = \frac{f}{f-\beta+1}\frac{LHV}{c_p T_{t2}}, \tag{24b}$$

$$\theta_{3y} - \theta_{3b} = \iota\left[\left(1+\delta\theta_S^3\right)\left(\theta_{S2}-\theta_{S1}\right) + \delta\mu_K\left(\theta_{S2}^4 - \theta_4^4\right)\right], \tag{24c}$$

$$\theta_{S1} - \theta_{3x} = \Delta_1, \tag{24d}$$

$$\theta_{3b} - \theta_{S2} = \Delta_2. \tag{24e}$$

The normalized temperature at Φ_{3a} is obtained from Eq. 6a. An additional equation is needed to obtain θ_4 in Eq. 24c, which is derived from a simple mass and energy balance of the combustor exit and dilution air streams

$$\theta_4 = \frac{\beta\theta_{3a} + (f-\beta+1)\,\theta_{3b}}{f+1}. \tag{25}$$

The non-dimensional parameters are defined as

$$\iota \equiv \frac{\lambda_S}{\dot{m}''_{3a} c_p l}, \qquad \delta \equiv \frac{16\sigma T_{t2}^3}{3K_R\lambda_S}, \qquad \mu_K \equiv \frac{3\varepsilon_K K_R\,(1-\epsilon)\,l}{16}, \tag{26}$$

where $\dot{m}''_{3a} = \dot{m}_{3a}/A_{CS}$. The parameters Δ_1 and Δ_2 represent the non-dimensional terminal temperature differences between Φ_{3x} and Φ_{S1} and between Φ_{3b} and Φ_{S2}, respectively, and are required for the finite porous matrix lengths considered by the second law of thermodynamics. In [34] it was shown that solid and gas-phase temperatures in a matrix-stabilized combustion system do not differ by more than 25K outside the reaction zone, and thus the analysis of Sec. 5 assumes that $\Delta_1 = \Delta_2 = 25\text{K}/T_{t2}$.

In the analysis of Sec. 5, the combustor is assumed to be perfectly adiabatic i.e. $\mu_K = 0$. The combustor exit temperature T_{3b} is thus constrained by the first law to the adiabatic flame temperature, expressed in non-dimensional form as

$$\theta_{3b} = \frac{(f-\beta+1)\,\theta_{3a} + \frac{fLHV}{c_p T_{t2}}}{f-\beta+1} \tag{27}$$

4.4. Discussion and Asymptotics of Non-dimensional Parameters and Equations

The ratio of solid to gas phase thermal transport is described by the parameter ι, which can be rewritten as

$$\iota = \frac{\lambda_S/l}{\rho\epsilon u_{pore}c_p}. \tag{28}$$

Variation in combustor mass flow rate $\dot{m}_{3a}$ affects ι only. The parameter δ captures the ratio of radiative to solid thermal conductivities, which is clear when it is rewritten as

$$\delta \sim \frac{\sigma T_{t2}^3/K_R}{\lambda_S}. \tag{29}$$

Internal radiative feedback is thus controlled by δ. Radiative heat losses are characterized by the product $\delta\mu_K$, as seen in Eq. 24. The parameter μ_K can be expressed as a ratio of the axial length of the porous matrix to the radiative attenuation length

$$\mu_K \sim \frac{(1-\epsilon)\,l}{1/\left(\varepsilon_K K_R\right)}. \tag{30}$$

The selection of $\mu_K = 0$ while $\delta > 0$ thus amounts to setting radiative losses to zero while allowing for internal radiative heat recirculation.

A brief asymptotic analysis of Eqs. 24 follows. Noting first that $\iota,\ \delta,\ \mu_K,\ \Delta_1,\ \Delta_2 \geq 0$ from their definitions, the case where $\mu_K = 0$ and $\Delta_1,\ \Delta_2 \to 0$ is considered for analysis, which represents an idealized porous matrix with no radiative heat losses and infinitesimal terminal temperature differences. In this case, $\theta_{S1} = \theta_{3x}$ and $\theta_{S2} = \theta_{3b}$, from which $\theta_S = (\theta_{3x} - \theta_{3b})/2$. Furthermore, the magnitudes of preheating and heat recirculation temperature changes become equivalent i.e. $\theta_{3x} - \theta_{3a} = \theta_{3y} - \theta_{3b}$. Equation 24a can thus be rewritten as

$$\frac{\theta_{3x} - \theta_{3a}}{\theta_{3b} - \theta_{3x}} = \iota\left(1 + \delta\theta_S^3\right). \tag{31}$$

In this form, it is evident that $\iota \to 0$ yields $\theta_{3x} = \theta_{3a}$ and hence $\theta_{3y} = \theta_{3b}$. The effect of the porous matrix diminishes to none, resulting in an internal temperature profile commensurate with no porous matrix being present. Furthermore, both the cases $\iota \to \infty$ and $\iota > 0,\ \delta \to \infty$ yield $\theta_{3x} = \theta_{3b}$, which represents the asymptotic limit of preheating achievable using matrix-stabilized combustion. In this limit, $\theta_{3y} = 2\theta_{3b} - \theta_{3a}$, where the value of θ_{3b} is derived in Eq. 27. Both the upper and lower asymptotic limits for matrix effectiveness are shown in Fig. 9a in the following section for the case where $\mu_K = 0$ but $\Delta_1,\ \Delta_2 > 0$.

5. Analysis of Porous Matrix-Integrated Brayton Cycle

The solution of Eqs. 24 yields a gaseous and solid temperature profile within the matrix as a function of upstream Brayton cycle parameters, ϕ and the non-dimensional parameters of Eq. 26. In all subsequent analysis, variation of ϕ is performed in tandem with π_c such that T_{t4} is maintained constant, as in Sec. 2. The values of ψ, ζ and ξ were held constant at the values of Table 1 unless noted otherwise.

Figure 9 shows that the model developed in Sec. 4 captures the key features of matrix-stabilized combustion, namely substantial gas preheating by the solid phase from Φ_{3a} to Φ_{3x}, resulting in a post-combustion temperature at Φ_{3y} in excess of the adiabatic flame temperature based solely on Φ_{3a}. The gas is subsequently cooled by the solid phase from Φ_{3y} to Φ_{3b}, exiting the porous matrix at the adiabatic flame temperature as required by the first law. Non-dimensional axial temperature profiles of the gas phase within the matrix are plotted in Fig. 9a for $\phi = \phi_0$ and a range of ι, showing the effect of the matrix in increasing the preheating and flame temperatures, where the curve for $\iota = 0$ corresponds to the base case without a porous matrix. The figure shows that the model correctly captures the base case temperature profile, such that no excess enthalpy combustion is achieved without a porous matrix. Furthermore, as $\iota \to \infty$, an asymptotic level of preheating is reached where $\theta_{3x} \approx \theta_{3b}$ and $\theta_{3y} \approx 2\theta_{3b} - \theta_{3a}$, which was predicted from the analysis of Sec. 4.4 for the ideal case where $\Delta_1,\ \Delta_2 \to 0$.

An example of a dimensional gaseous temperature profile within the porous matrix is shown in Fig. 9b. The set of mechanical and radiative porous matrix properties $\chi = [\lambda_S, l, \epsilon, \varepsilon_K, K_R, d_{PH}, d_{RC}]^T$ was selected based on those used in previous numerical and experimental studies [12],

$$\chi = \left[8.7\mathrm{W/(m \cdot K)}, 76.2\mathrm{mm}, 0.8, 0.9, 0.686\mathrm{m}^{-1}, 0.39\mathrm{mm}, 2.54\mathrm{mm}\right]^T,$$

where d_{PH} and d_{RC} are the pore diameters of the preheating and recirculation segments, respectively. The value of K_R employed represents the average of those obtained for the two matrix segments, and ε_K was taken from [35] for silicon carbide. Assuming $\mu_K = 0$, and using the mass flux of Sec. 3.2, $\iota \approx 0.05$ and $\delta \approx 1.38$. The effect of the Brayton cycle can be seen in the increase of T_{t3a} with decreasing ϕ; this effect alone was shown in Sec. 3.1 to be insufficient for stabilizing combustion below ϕ_0.

5.1. Pressure Drop in Matrix-Stabilized Combustion

A matrix-stabilized combustor does not require the turbulent swirling flow field most combustor designs [3] employ for flame stabilization and therefore does not incur the associated pressure drop. Instead, frictional losses are incurred from flow through the porous matrix, as governed by the Darcy-Forchheimer equation [36]

$$\frac{dp}{dx} = -\frac{RT}{p}\left(\frac{\mu(T)}{K_1}\dot{m}'' + \frac{1}{K_2}\dot{m}''^2\right) \tag{32}$$

where x is the bulk flow direction, $\mu(T)$ is the temperature-dependent dynamic viscosity and ideal gas behavior has been assumed. The constants K_1 and K_2 are the intrinsic permeability and the non-Darcian drag coefficient, which are functions of the matrix geometry [37]. Since Eq. 32 is a function of temperature both explicitly and through μ, it cannot be integrated without the complete axial temperature profile in the porous matrix $T(x)$, which is not available from the current thermodynamic analysis.

It has been shown experimentally and through numerical simulation in [12] that the pressure drop due to matrix-stabilized combustion does not exceed 2.5% for the matrix properties χ of Sec. 5 and mass flux of

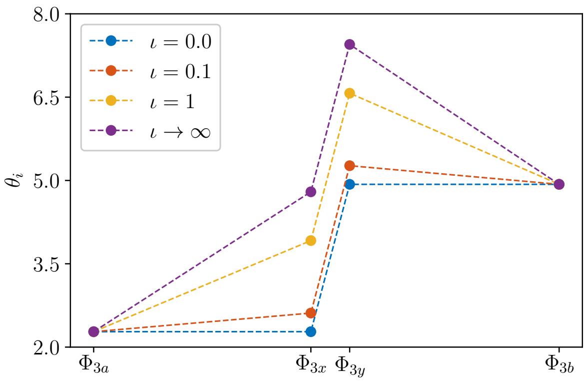

(a) Non-dimensional temperature profile, $\phi = 0.3$, $\delta = 0.01$, $\mu_K = 0$

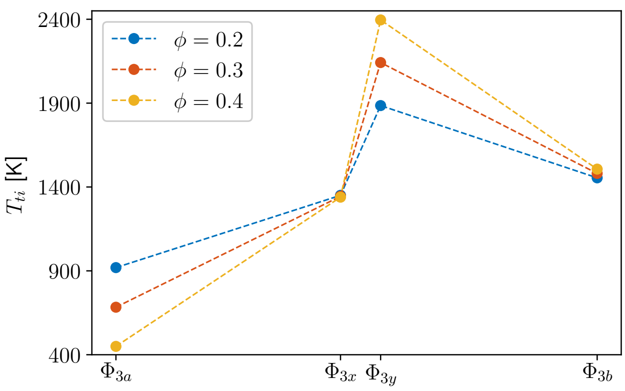

(b) Dimensional temperature profile, $\iota = 0.05$, $\delta = 1.38$, $\mu_K = 0$

Figure 9: Gas phase temperature profiles for matrix-stabilized combustion: (a) non-dimensional temperature profiles for parametric variations in thermal transport parameter ι and (b) dimensional temperature profiles for variations in equivalence ratio ϕ. Abscissa gives thermodynamic states in porous matrix but does not provide a length scale. Dashed lines are for visualization and do not imply a particular temperature profile between states.

Sec. 3.2 at atmospheric conditions. Recent experiments using similar matrix properties and mass flux values performed at pressures of up to 8bar exhibited even lower combined pressure losses [38]. For the purposes of this analysis, it is conservatively assumed that the pressure drop across the matrix is constant at 5% such that $\pi_b = \pi_{PH}\pi_{CB}\pi_{RC} = 0.95$, where π_{PH} and π_{RC} are the frictional pressure loss ratios in the preheating and recirculation segments, and π_{CB} is the Rayleigh loss due to combustion.

5.2. Open Brayton Cycle with Matrix-Stabilized Combustion

Analysis analogous to that of Sec. 2.2 is performed for a Brayton cycle employing matrix-stabilized combustion. From the first law of thermodynamics, so long as combustion remains locally fuel-lean such that Eq. 2 holds, then Eqs. 6 also hold. For a given set of parameters $\{\Phi_2, \phi, \psi, \zeta, \xi\}$, the specific combustion process cannot affect the post-combustion state Φ_{3b}. Rather, the use of matrix stabilization changes the range of accessible parameters given combustor stability considerations. The effect of matrix-stabilized combustion on the Brayton cycle considered in Sec. 2 is shown in Fig. 10.

From Fig. 10a, it is evident that for the same ϕ, the Brayton cycle employing matrix stabilization has a maximum temperature in excess of the combustor exit temperature T_{t3b}, to which the preheated gas temperature T_{t3x} is comparable. Figure 10b illustrates the effects of matrix stabilization on pressure, namely the pressure loss across the preheating section, followed by isobaric heat addition in the thin combustion zone and pressure loss across the recirculation section. Figure 10 therefore represents the major changes to the Brayton cycle brought about by matrix-stabilized combustion, namely the creation of a preheated state Φ_{3x} and an excess-enthalpic combusted state Φ_{3y}.

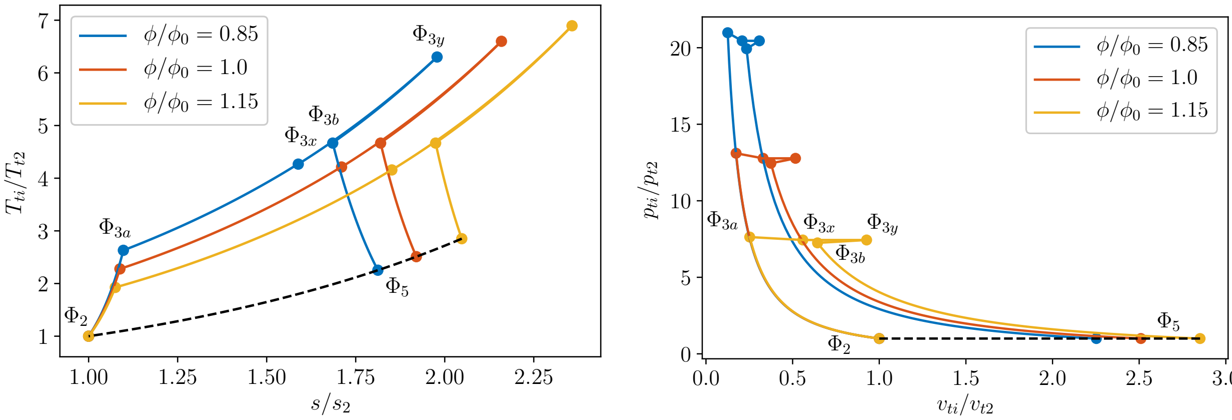

(a) $T-s$ diagram with matrix-stabilized combustion

(b) $p-v$ diagram with matrix-stabilized combustion

Figure 10: Effect of changing global equivalence ratio ϕ while maintaining a constant turbine inlet temperature T_{t4} on open Brayton cycle with matrix-stabilized combustion, $\beta = 0$, $\pi_b = \pi_{PH}^2 = \pi_{RC}^2 = 0.95$, $\zeta = \{0.9, 0.9, 0.95\}$, $\iota = 0.05$, $\delta = 1.38$, $\mu_R = 0$.

5.3. Preheating Temperature and LFL

The most important effect of the porous matrix on the thermodynamic cycle is the preheating of the reactants to T_{t3x}, as this results in the reduction of LFL as per Eq. 11. The dependence of T_{t3x} on ι and δ can be seen in Fig. 11a, showing that the greater the effectiveness of the porous matrix, the greater the level of reactant preheating. As was described in Sec. 3.1, LFL for methane is determined uniquely by the unburned gas temperature for a large range of pressures. The empirical correlation of Eq. 11 can be rewritten as the ratio of $X_{f,LFL}$ achieved with matrix-stabilized combustion to the reference condition of Sec. 2 using Eq. 12, since ϕ_0 is assumed to be at the lean limit, as in Sec. 3.1. Solving for the lean limit global equivalence ratio that is achieved at Φ_{3x} through matrix-stabilized combustion ϕ_{min}, the following expression is obtained in terms of T_{t3x}

$$\frac{\phi_{min}}{\phi_0} = \frac{(1-\beta)}{1-\beta+\phi_0 \tilde{f}_{st}} \left(\frac{T_{t3x}}{T_{t3a,0}}\right)^{-n} \left[1 - \frac{\phi_0 \tilde{f}_{st}}{1-\beta+\phi_0 \tilde{f}_{st}} \left(\frac{T_{t3x}}{T_{t3a,0}}\right)^{-n}\right]^{-1} \tag{33}$$

where $T_{t3a,0}$ is T_{t3a} obtained from Eq. 6a for $\phi = \phi_0$. From Eq. 24, however, T_{t3x} is itself a function of ϕ. Thus, Eq. 33 can be solved iteratively together with Eq. 24 to obtain ϕ_{min} as a function of ι and δ, the results of which are plotted in Fig. 11b. As expected from Fig. 11a, LFL is reduced with increasing porous matrix effectiveness, with lean limit extension reaching an asymptotic limit of approximately $\phi_{min}/\phi_0 \approx 0.68$. For $\phi_0 = 0.3$, this amounts to an extension of the combustor LFL by 32%. Figure 11b clearly shows that, for a wide range of operating conditions and matrix properties, matrix-stabilized combustion does in fact reduce LFL below that achievable without heat recirculation, and can thus be used to achieve the efficiency gains obtained from leaner engine operation. It is further noted that the lowest ϕ_{min} achieved using matrix-stabilized combustion is greater than the autoignition limit described in Sec. 3.2, and thus the lean limit extension will not result in autoignition at Φ_{3a}, assuming that the preheating section is designed with sufficiently small pores such that flame propagation due to autoignition is inhibited by thermal quenching [11].

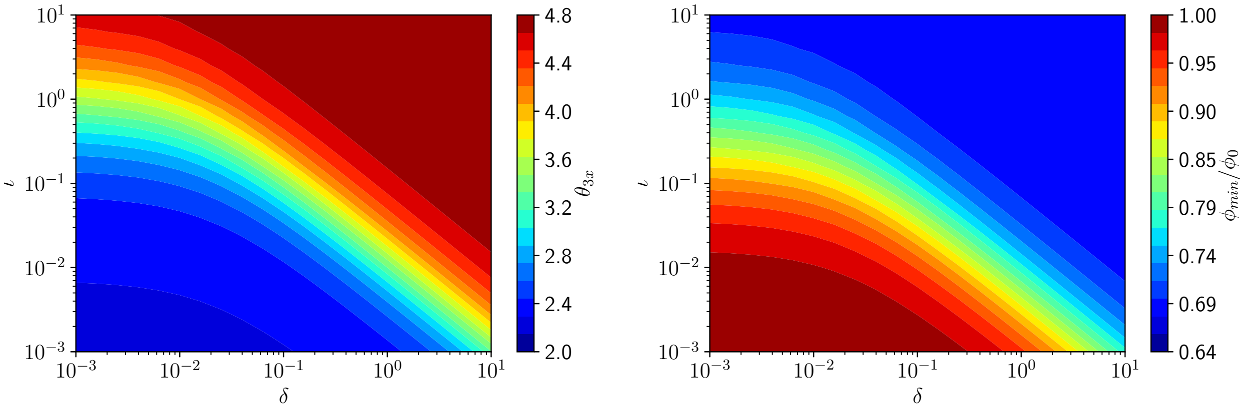

(a) Non-dimensional preheating temperature, θ_{3x}, at $\phi/\phi_0 = 1$

(b) Lean flammability limit achieved with matrix-stabilized combustion

Figure 11: Parametric variation of matrix-stabilized combustion system behavior with porous matrix design parameters ι and δ with $\mu_K = 0$.

5.4. *Effect of Matrix-Stabilized Combustion on Cycle Thermal Efficiency and Emissions*

As was discussed in Sec. 2 and shown in Fig. 4a, reduction in ϕ while maintaining constant T_{t4} results in improved η_{th}. The results shown in Fig. 11b were used to obtain a map of η_{th} as a function of matrix parameters and turbomachinery efficiencies. For a given set of matrix parameters ι and δ, ϕ_{min} was obtained, the corresponding η_{th} was calculated for a given set of η_c and η_t, and was normalized by the corresponding nominal efficiency $\eta_{th,0}$ obtained at ϕ_0. The results of this are shown in Fig. 12. Application of matrix-stabilized combustion to the Brayton cycle considered was found to result in improvements in cycle efficiency of up to $\eta_{th}/\eta_{th,0} = 1.2$ in the case of isentropic turbomachinery. This corresponds to an absolute improvement of 11% compared to the nominal design considered due to lean limit extension. For non-ideal turbomachinery efficiencies $(\eta_c, \eta_t) = (0.9, 0.9)$, an improvement of of up to $\eta_{th}/\eta_{th,0} = 1.06$ was obtained, corresponding to a 2.5% efficiency gain compared to the nominal design. In the case of non-ideal turbomachinery efficiencies, the maximum gain in η_{th} occurs along a finite contour of matrix parameter values due to the efficiency maximum of the non-ideal system with reducing ϕ, seen in Fig. 4a. This is in contrast to the case of isentropic turbomachinery, where the maximum efficiency gain occurs at the asymptotic limit of lean flammability limit reduction with increasing porous matrix effectiveness, as can be seen by comparing Fig. 11b and Fig. 4a. These results show that for an engine employing a matrix-stabilized combustion system, the porous matrix and engine turbomachinery can be designed in tandem such that for a given operating condition, an optimal reduction in LFL and thereby a maximum increase in η_{th} is obtained.

The effect of operating at a reduced ϕ using a matrix-stabilized combustion system on NO_x and CO emissions requires spatial resolution of the interactions between gas and solid phases beyond the thermodynamic treatment given in this study. The formation of these pollutants is highly dependent on residence time in zones of elevated temperature [39]. It has been shown experimentally that matrix-stabilized combustion results in low NO_x and CO emissions in gas turbine engines [13] and that these can be further diminished by reducing ϕ at constant pressure due to reduced residence times [11]. When maintaining a constant T_{t4}, Fig. 5 shows that reduced ϕ with increased combustor inlet temperatures and pressures result in reduced emissions in lean premixed combustors not employing matrix-stabilization. These results, however, do not take into account the preheating and quenching effects of the porous matrix, to which NO_x and CO emissions are sensitive. Emission profile measurements in recent experiments of matrix stabilized combustion at elevated pressures and reactant temperatures have been shown to support these trends [38], with significant reductions in NO_x emissions with reduction ϕ. Quantitative discussion of emissions profiles, however, requires detailed simulations and further experimental analysis beyond the scope of this study.

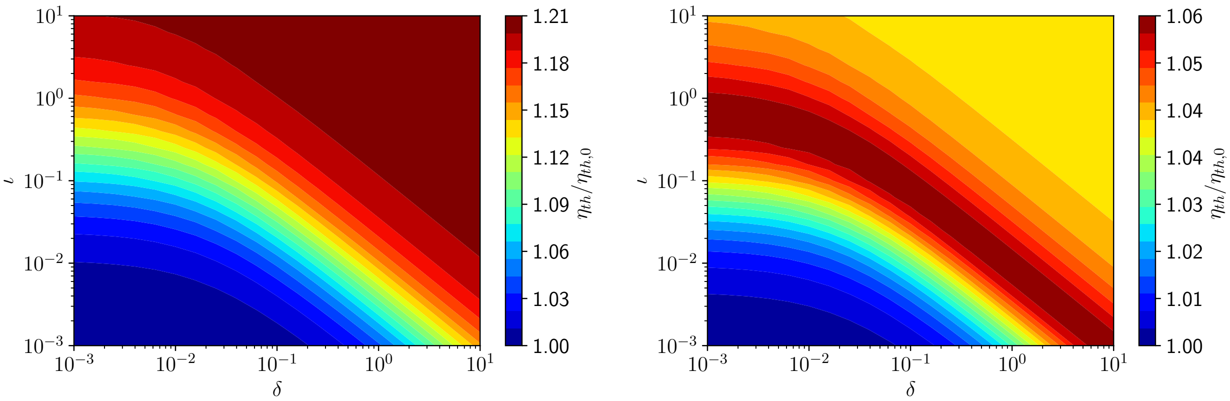

(a) $\eta_c = 1$, $\eta_t = 1$

(b) $\eta_c = 0.9$, $\eta_t = 0.9$

Figure 12: Effect of applying matrix-stabilized combustion to a Brayton cycle on thermal efficiency η_{th} as a function of porous matrix design parameters ι and δ, with $\mu_K = 0$.

6. Discussion

6.1. Efficiency versus Specific Work

Although this analysis has focused on η_{th}, engine designers must also consider the air-mass-specific net work $w \equiv \dot{W}_{net}/\dot{m}_2$. Since engines are generally designed to produce a certain power output, a reduction in w results in a need for larger turbomachinery with greater air throughput to achieve the same power. Though less critical in stationary power generation, engine size (and consequently weight) is a key factor in aerospace propulsion. From Eqs. 2 and 4,

$$w = \eta_{th} \phi f_{st} LHV, \tag{34}$$

which for a constant ψ, ζ and ξ is uniquely a function of ϕ. The variation of w with ϕ is shown in Fig. 13. The dependence of η_{th} on ϕ is expressed in Eq. 7 and illustrated in Fig. 4a, which shows that a reduction in ϕ results in an increase in η_{th}. Thus, in Eq. 34, the effects of reduced ϕ and improved η_{th} are in competition.

Figure 13 shows the effect of reduced ϕ on w. From the figure, it is evident that although the proposed reduction in ϕ results in efficiency gains, these gains would have to be realized through a larger engine due to reduced specific work. However, the dependence of w on ϕ is non-monotonic, and thus with careful selection of the cycle parameters, the ϕ for which w is a maximum can be modulated to lessen the reduction in w incurred.

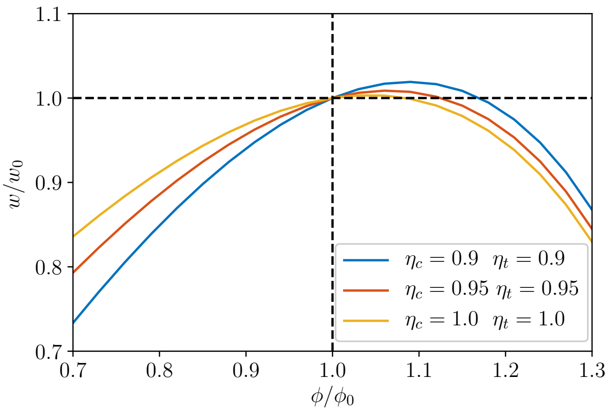

Figure 13: Effect of changing global equivalence ratio ϕ while maintaining a constant turbine inlet temperature T_{t4} on cycle air-mass-specific net work w.

6.2. Efficiency versus Pressure Losses

As was noted in Sec. 5.1, quantitative consideration of pressure drop requires spatial resolution of the flow field, and thus the present discussion of the effect of pressure drop on efficiency is limited to a qualitative one. Considering Eq. 32, for a constant mass flux, increased temperatures in the matrix result in increased frictional losses due to the temperature dependence of the coefficient RT/p as well as that of viscosity. The pressure drop across the combustor Δp can be estimated as $\Delta p \sim -l \cdot dp/dx$, showing that frictional losses increase with matrix axial length. However, from Eq. 26 it can be seen that reduction in axial length results in an increased matrix effectiveness since $\iota \sim 1/l$, thus increasing gas temperatures within the matrix, but allowing operation at leaner equivalence ratios at higher pressure ratios. It is also clear from Eq. 32 that

$dp/dx \sim -1/p$, and pressure losses in matrix-stabilized combustion are therefore expected to reduce with increasing combustor inlet pressure. This has been shown experimentally [38] for methane and heptane fuels at pressures up to 20bar. The design and optimization of a matrix-integrated Brayton cycle, therefore, requires the simultaneous consideration of the effects on η_{th} due to losses from Δp and gains due to operation at a reduced ϕ.

6.3. *Efficiency versus Radiative Heat Losses*

Throughout this work, the effect of heat losses on η_{th} have been neglected. Although this assumption is reasonable for conductive and convective heat losses in a conventional Brayton cycle analysis, heat losses in matrix-stabilized combustion arising from solid radiation can be considerable if steps for its mitigation are not taken, and are quantified for axial heat losses arising at the ends of the matrix using the parameter μ_K in Sec. 4. This section seeks to quantify the critical level of radiative heat loss which results in the superadiabatic system no longer providing improvement in η_{th}. It is assumed that no steps to mitigate radiative heat losses were taken. From Eq. 23, the mass-specific total radiative heat loss $q_{loss} = \dot{Q}_{loss}/\dot{m}_{3a}$ is written in non-dimensional form as

$$\Xi_{loss} = \iota\delta\mu_K \left[\left(\theta_{S1}^4 - \theta_{3a}^4\right) + \left(\theta_{S2}^4 - \theta_4^4\right)\right] \tag{35}$$

where $\Xi_{loss} = q_{loss}/(c_p T_{t2})$. From Eq. 35 it is clear that for a given set of matrix effectiveness parameters ι and δ, radiative heat losses are directly proportional to μ_K, with matrix temperatures functions of μ_K through Eqs. 24.

Radiative heat losses affect η_{th} in two ways. Firstly, heat losses reduce the product stream temperature exiting the combustor. The effect of this temperature reduction on η_{th} is clear from Eq. 7, namely any reduction in T_{t4} directly reduces efficiency, as was noted in Sec. 2.3. Secondly, the heat losses reduce the amount of heat available for recirculation and hence reduce reactant preheating. This reduces LFL extension, and thereby reduces efficiency. Here the combined effect is considered, namely by determining the level of radiative heat loss, quantified by μ_K, which eliminates any increase in η_{th} attained through matrix-stabilized combustion, expressed as $\mu_K|_{\eta_{th}=\eta_{th,0}}$. This is done for engine cycles which were initially optimized through lean limit extension for given values of ι and δ when neglecting heat losses. Figure 14 shows the effect of radiative heat losses as a function of ι and δ for both non-ideal and ideal turbomachinery. In both cases, the figure shows that radiative heat losses are strongly dependent on both ι and δ, although dependence on ι is less significant at small values of δ. Of practical relevance is that with increasing matrix effectiveness and thus lean limit extension, efficiency gains become more sensitive to μ_K, with values as small as $\mu_K \sim 10^{-4}$ sufficient to eliminate efficiency gains for $(\iota, \delta) \sim (1, 1)$. Thus, the design of a gas turbine Brayton cycle taking advantage of the increased efficiency achievable through lean limit extension using matrix stabilized combustion must carefully consider the effects of solid radiation from the matrix, including measures to minimize it.

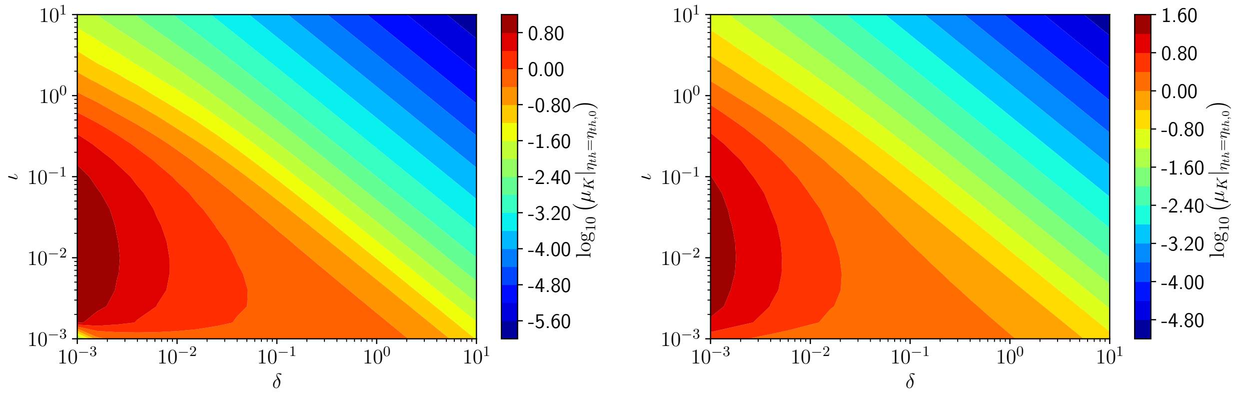

(a) $\eta_c = 0.9$, $\eta_t = 0.9$

(b) $\eta_c = 1$, $\eta_t = 1$

Figure 14: Effect of radiative heat losses on Brayton cycle thermal efficiency as a function of porous matrix design parameters ι and δ. $\mu_K|_{\eta_{th}=\eta_{th,0}}$ denotes the level of radiative heat loss, parametrized by μ_K, which results in no efficiency gain relative to the nominal cycle i.e. $\eta_{th} = \eta_{th,0}$.

6.4. Practical Considerations

The effect of combustion product stream dilution on η_{th} was not considered in Eq. 7, and the dilution ratio β was considered constant in this work. However, the reduction of β results in a reduction in the local combustor equivalence ratio as per Eq. 3. Given that engines are designed to operate near LFL, reactant preheating would be required to stabilize a combustion system with reduced dilution. As with the reduction in global equivalence ratio, this is achievable using matrix-stabilized combustion. The reduction of β would then result in reduced stagnation pressure losses due to the flow of cooling air through combustor liner holes, improving η_{th}, and could be quantified through a more detailed analysis.

The analysis of Sec. 5 assumed that the combustor was adiabatic, and thus $\mu_K = 0$ in the matrix-stabilized combustion model. Section 6.3 showed the significance of radiative heat losses for thermal efficiency in the matrix-stabilized system. Such heat losses can also be detrimental to the components near the porous matrix due to increased thermal loading and associated material degradation. Engine designs must therefore seek to mitigate radiative losses from the matrix, and furthermore must take into account the effect of incident thermal radiation on the longevity of components within the engine exposed to the matrix.

In Sec. 3, two modes of combustor instability were considered, namely flame-out at the lean flammability limit and flashback due to autoignition. In the design of combustion systems, dynamic modes of instability due to thermoacoustics are a key concern. Thermoacoustic instability in swirl-stabilized combustion chambers has been shown to be reduced by the use of porous inserts within the combustion chamber [40]. In one configuration tested experimentally, fully matrix-stabilizated combustion was found to reduce the propensity for thermoacoustic instability [13], but further study is necessary to definitively assess this effect.

Finally, the proposed reduction in ϕ and increase in π_c result in a significant increase in T_{t3} according to Eq. 6a. Such high pressures and temperatures may lead to hardware difficulties. Greater mechanical stress would be placed on engine components and coking may occur on nozzles, issues which would have to be mitigated in the design process.

7. Conclusions

A system-level thermodynamic analysis of the effects of fuel-air equivalence ratio on the performance of a gas turbine engine operating according to an open Brayton cycle was performed. It was shown that reduction in ϕ results in efficiency gains when turbine inlet temperature is held constant and pressure ratio is increased. However, it was further shown that redesigning engine cycles in this manner is inhibited by combustion stability considerations, specifically that of flame-out due to operation below LFL for premixed combustion. Matrix-stabilized combustion was proposed as a means of preheating fuel-air mixtures to achieve flammability and thereby to extend LFL and enable more efficient cycle performance. A novel thermodynamic model of combustion in porous media was developed, and was used in conjunction with a Brayton cycle analysis to quantify the expected gains in efficiency. Key results of the analysis include:

- Matrix-stabilized combustion enables the extension of LFL due to heat recirculation parametrized by non-dimensional groups of matrix properties ι, δ and μ_K, defined in Eq. 26
- Combustion stability in a porous matrix at LFL is controlled by the preheating temperature T_{t3x}, a function of the heat recirculation within the matrix
- Cycle efficiency can be improved significantly through matrix-stabilized combustion due to its reduction of LFL, relaxing the restriction on ϕ and thereby allowing for a higher π_c and lower β
- For the engine parameters considered, matrix-stabilized combustion is shown to result in efficiency gains of up to 11% and extension of LFL by up to 32% while enabling reduced emissions of NO_x and CO

Future work includes the extension of the analysis to advanced turbofan engines employing lean premixed combustion, as well as detailed comparison of the results of the matrix-stabilized combustion model with the results of atmospheric and high-pressure experiments and simulations. With regard to the practical application of this concept in gas turbine engines, demonstration of the durability of the matrix material is a key requirement. Further cycle efficiency improvements may be obtained through the variation of the relative lengths of the matrix sections to minimize pressure drop while maintaining combustion stability, and may be used in conjunction with high-pressure matrix-stabilized combustion emission data in cycle design.

8. Acknowledgements

This work is supported by a Leading Edge Aeronautics Research for NASA (LEARN) grant (No. NNX15AE42A).

9. References

[1] M. Jarre, M. Noussan, A. Poggio, Operational analysis of natural gas combined cycle CHP plants: Energy performance and pollutant emissions, Applied Thermal Engineering 100 (2016) 304–314.

[2] M. M. Schorr, J. Chalfin, GE Power Generation gas turbine NOx emissions approaching zero is it worth the price?, Technical Report, GE Power Systems, 1999.

[3] A. Lefebvre, D. Ballal, Gas Turbine Combustion, CRC Press, 2010.

[4] C. T. Chang, C.-M. Lee, J. T. Herbon, S. K. Kramer, NASA environmentally responsible aviation project develops next-generation low-emissions combustor technologies (Phase I), Journal of Aeronautics & Aerospace Engineering 2 (2013) 1–10.

[5] D. Hardesty, F. Weinberg, Burners producing large excess enthalpies, Combustion Science and Technology 8 (1973) 201–214.

[6] L. Catoire, V. Naudet, Estimation of temperature-dependent lower flammability limit of pure organic compounds in air at atmospheric pressure, Process Safety Progress 24 (2005) 130–137.

[7] T. Takeno, K. Sato, An excess enthalpy flame theory, Combustion Science and Technology 20 (1979) 73–84.

[8] S. Panigrahy, S. C. Mishra, The combustion characteristics and performance evaluation of DME (dimethyl ether) as an alternative fuel in a two-section porous burner for domestic cooking application, Energy 150 (2018) 176–189.

[9] H. Wu, M. Kaviany, O. Kwon, Thermophotovoltaic power conversion using a superadiabatic radiant burner, Applied Energy 209 (2018) 392–399.

[10] J. L. Ellzey, E. L. Belmont, C. H. Smith, Heat recirculating reactors: Fundamental research and applications, Progress in Energy and Combustion Science 72 (2019) 32–58.

[11] D. Trimis, F. Durst, Combustion in a porous medium-advances and applications, Combustion Science and Technology 121 (1996) 153–168.

[12] S. Sobhani, D. Mohaddes, E. Boigne, P. Muhunthan, M. Ihme, Modulation of heat transfer for extended flame stabilization in porous media burners via topology gradation, Proceedings of the Combustion Institute 37 (2019) 5697–5704.

[13] E. Noordally, J. M. Przybylskil, J. J. Witton, Porous media combustors for clean gas turbine engines, Technical Report, Cranfield University, 2004.

[14] M. A. Mujeebu, M. Zulki, A. A. Mohamad, M. Z. A. Bakar, Trends in modeling of porous media combustion, Progress in Energy and Combustion Science 36 (2010) 627–650.

[15] M. M. Ehsan, S. Duniam, J. Li, Z. Guan, H. Gurgenci, A. Klimenko, Effect of cooling system design on the performance of the recompression CO2 cycle for concentrated solar power application, Energy 180 (2019) 480–494.

[16] S. Sobhani, Computational and Experimental Investigation of Flow and Combustion Physics in Porous Media, Ph.D. thesis, Stanford University, 2019.

[17] J. D. Mattingly, Elements of Propulsion: Gas Turbines and Rockets, AIAA, 2000.

[18] J.-C. Han, S. Datta, S. Ekkad, Gas Turbine Heat Transfer and Cooling Technology, CRC Press/Taylor & Francis, 2013.

[19] Gas Turbine Portfolio, Technical Report, Siemens AG, Erlangen, Germany, 2017. Article No. PGDG-B10006-06-7600.

[20] H. Saravanamuttoo, G. Rogers, H. Cohen, Gas Turbine Theory, Pearson Education Ltd., 2001.

[21] D. G. Goodwin, H. K. Moffat, R. L. Speth, Cantera: An object-oriented software toolkit for chemical kinetics, thermodynamics, and transport processes, 2017. Available from `http://www.cantera.org`.

[22] G. P. Smith, D. M. Golden, M. Frenklach, N. W. Moriarty, B. Eiteneer, M. Goldenberg, C. T. Bowman, R. K. Hanson, S. Song, W. C. Gardiner, Jr., V. V. Lissianski, Z. Qin, GRI-Mech 3.0, 2000. Available from http://www.me.berkeley.edu/gri-mech/.

[23] L. Esclapez, P. C. Ma, E. Mayhew, R. Xu, S. Stouffer, T. Lee, H. Wang, M. Ihme, Fuel effects on lean blow-out in a realistic gas turbine combustor, Combustion and Flame 181 (2017) 82–99.

[24] M. Hertzberg, K. L. Cashdollar, I. A. Zlochower, Flammability limit measurements for dusts and gases: Ignition energy requirements and pressure dependences, Symposium (International) on Combustion 21 (1988) 303–313.

[25] S. Kondo, A. Takahashi, K. Takizawa, K. Tokuhashi, On the pressure dependence of flammability limits of CH2=CFCF3, CH2F2 and methane, Fire Safety Journal 46 (2011) 289–293.

[26] S. Plee, A. Mellor, Review of flashback reported in prevaporizing/premixing combustors, Combustion and Flame 32 (1978) 193–203.

[27] J. Fritz, M. Kroener, T. Sattelmayer, Flashback in a swirl burner with cylindrical premixing zone, Journal of Engineering for Gas Turbines and Power 126 (2004) 276.

[28] M. Foust, D. Thomsen, R. Stickles, C. Cooper, W. Dodds, Development of the GE Aviation low emissions TAPS combustor for next generation aircraft engines (2012). AIAA Paper 2012-0936.

[29] C. K. Law, Combustion Physics, Cambridge University Press, 2006.

[30] S. Sobhani, B. Haley, D. Bartz, J. Dunnmon, J. Sullivan, M. Ihme, Investigation of lean combustion stability, pressure drop, and material durability in porous media burners (2017). ASME Paper GT2017-63204.

[31] C. Bedoya, I. Dinkov, P. Habisreuther, N. Zarzalis, H. Bockhorn, P. Parthasarathy, Experimental study, 1D volume-averaged calculations and 3D direct pore level simulations of the flame stabilization in porous inert media at elevated pressure, Combustion and Flame 162 (2013) 3740–3754.

[32] E. Placido, M. C. Arduini-Schuster, J. Kuhn, Thermal properties predictive model for insulating foams, Infrared Physics and Technology 46 (2005) 219–231.

[33] P.-F. Hsu, J. R. Howell, Measurements of thermal conductivity and optical properties of porous partially stabilized zirconia, Experimental Heat Transfer 5 (1992) 293–313.

[34] C. Zheng, L. Cheng, A. Saveliev, Z. Luo, K. Cen, Gas and solid phase temperature measurements of porous media combustion, Proceedings of the Combustion Institute 33 (2011) 3301–3308.

[35] G. Neuer, Spectral and total emissivity measurements of highly emitting materials, International Journal of Thermophysics 16 (1995) 257–265.

[36] K. Vafai, Handbook of Porous Media, Marcel Dekker, 2000.

[37] S. Ergun, A. Orning, Fluid Flow through Randomly Packed Columns and Fluidized Beds, Industrial & Engineering Chemistry 41 (1949) 1179–1184.

[38] S. Sobhani, J. Legg, D. F. Bartz, J. J. Kojima, C. T. Chang, J. D. Sullivan, J. P. Moder, M. Ihme, Experimental investigation of lean premixed pre-vaporized liquid-fuel combustion in porous media burners at elevated pressures up to 20 bar, Combustion and Flame 212 (2020) 123–134.

[39] D. A. Sullivan, A simple gas turbine combustor NOx correlation including the effect of vitiated air, Journal of Engineering for Power (1977) 145–152.

[40] D. L. Depperschmidt, J. A. Kornegay, J. C. Allen, A. K. Agrawal, Effect of preheating on flame structure of a swirl stabilized combustor with porous insert to control thermoacoustics (2016). ASME Paper GT2016-58064.